

## A switched current controller with commutation delay compensation for the reduction of commutation torque ripple in BLDCM drives

Türker TÜRKER<sup>1,\*</sup>, Ihsan Obayes Khudhair KHUDHAIR<sup>2</sup>

<sup>1</sup>Department of Control & Automation Engineering, Yıldız Technical University, İstanbul, Turkey

<sup>2</sup>State Company for Tires Ind., Najaf, Iraq

Received: 07.06.2016

Accepted/Published Online: 02.10.2016

Final Version: 30.07.2017

**Abstract:** The mathematical model of the equivalent circuit of a brushless DC motor switches during the operation due to commutation. This issue causes a sudden ripple in the output torque, which is called commutation torque ripple. Brushless DC motor drives suffer from commutation torque ripple, affecting the performance of the motor in practical applications. A discrete-time switched controller is proposed to reduce the commutation torque ripple in brushless DC motor drives. The proposed controller is a combination of two distinct controllers designed for two different working regions of brushless DC motors. In addition, the commutation delay is also considered in the controller and a predictive structure is implemented to reduce this effect. The overall control scheme consisted of the switched controller and the commutation delay compensation, showing the originality of this study. The performance of the proposed controller scheme is tested through various comprehensive experiments to illustrate its effectiveness and viability.

**Key words:** Brushless DC motor, commutation torque ripple, switched control, commutation delay compensation

### 1. Introduction

Use of permanent magnet motors (PMMs) is increasing gradually due to their advantages such as efficiency, higher power density, higher torque density, and reliability. PMMs are especially preferred for applications requiring large and smooth torque output, light weight, small size, and quick response in areas including robotics, home appliances, and medical and military applications.

PMMs may be taken into consideration as two main groups: permanent magnet synchronous motors (PMSMs) and brushless direct current motors (BLDCMs). The main difference between them is the form of the ideal back-electromotive force (emf) signals, which are sinusoidal in PMSMs and trapezoidal in BLDCMs. Thus, PMSMs are driven by sinusoidal phase currents while BLDCMs require square-wave-like phase currents for ripple-free output torque. Having a simpler drive scheme compared to that for PMSMs is the main advantage of BLDCMs. However, this simplicity introduces probably the worst drawback to BLDCM drives, namely commutation torque ripple. Commutation torque ripple is caused by the fact that the phase currents cannot have ideal rectangular shape, although phase back-emf signals are assumed to be trapezoidal. This kind of torque ripple restricts the application area of BLDCMs especially for applications requiring high performance and smooth torque output.

Back-emf signals are assumed to be trapezoidal with 120° difference between phases in many studies concerning the reduction of commutation torque ripple [1–9]. In this case, outgoing phase back-emf starts

\*Correspondence: [turker@yildiz.edu.tr](mailto:turker@yildiz.edu.tr)

decaying at the beginning of the commutation period. However, back-emf signals of incoming and outgoing phases are assumed to be constant during the commutation period in many works [4–9] due to the short duration of the commutation period. This assumption allows analytical analysis of the commutation period and commutation torque ripple [6–9]. The analytical analysis with the aforementioned assumptions asserts that if slew rates of incoming and outgoing currents are inversely identical, commutation torque ripple is eliminated. Accordingly, various PWM modification techniques are proposed in the literature in order to achieve equal slew rates for incoming and outgoing currents. A detailed analysis of commutation torque ripple is carried out in [8], and three different methods are implemented to eliminate commutation torque ripple after the desired phase current trajectories are obtained. In [4], the modification of PWM signal is performed by dividing a switching period into three segments where each has its own role in eliminating commutation torque ripple. Similarly, Salah et al. [7] propose another modified PWM approach in which PWM duties are computed for conduction and commutation periods and for high and low speeds separately. The duration of the commutation period is a key parameter in such approaches and it has to be known precisely to provide equal slew rates. A circuit is designed and utilized in [5] for the calculation of commutation time; then a modification of PWM is implemented to reduce commutation torque ripple. It is worth mentioning that PWM duty ratio is computed directly as a result of analytical analysis in these works, and hence the control structure becomes fragile. As a matter of fact, the proposed PWM modification methods are highly sensitive to parametric uncertainties in the model parameters, unmodelled dynamics, and disturbances.

On the other hand, commutation torque ripple reduction methods are also proposed for BLDCMs with nonideal back-emfs. In this case, back-emf signals are measured either before or during the operation. Then this information is utilized in the control structure. Similar to the ideal back-emf case, it is possible to calculate the settling time of incoming and outgoing currents approximately [10], so that PWM duty for the reduction of commutation torque ripple can be determined. A detailed analysis of commutation torque ripple for nonideal back-emf case is carried out in [11]. In addition, the effect of commutation angle error on commutation torque ripple caused by misalignment of Hall effect sensors is examined and a method is proposed to reduce this effect.

Apart from the aforementioned methodologies, various controller types are also implemented to reduce commutation torque ripple in BLDCM drives. The dead-beat controller is applied to reduce commutation torque ripple in BLDCM drives with nonideal back-emfs [12]. Since all the model parameters are required to apply the dead-beat controller, a priori knowledge on phase back-emf signals is provided in the study. In order to apply the optimal switching state for the reduction of commutation torque ripple, a finite state model predictive controller is proposed [9]. However, the BLDCM model is considered to be known exactly in this model predictive control approach, which is usually not possible. Despite the variable switching frequency, direct torque control is another advantageous approach for torque ripple reduction in BLDCM drives [3,13]. Particularly, a direct torque control approach is applied via a four-switch inverter in [13]. Another method proposed for the reduction of commutation torque ripple in BLDCM drives is to regulate DC link voltage of the inverter instead of applying PWM signals to the switches for chopping [11,14]. This method provides good results in some cases, but it requires an additional circuit in the drive. Recently, an interesting method regulating output torque by controlling the input energy is presented in [15]. Although the exact model is not required, efficiency of the drive has to be known precisely and sensitive numerical integration of measured quantities plays an important role in that work. On the other hand, since the switching between conduction and commutation periods may occur at any point in a PWM period, a time lag exists between the beginning point of commutation and the following PWM period. This time lag is called commutation delay and it has

a significant adverse effect on commutation torque ripple. Minimization of this effect is provided by a hybrid combination of PWM switching and adjustable DC link voltage methods in [16].

This paper aims to reduce commutation torque ripple in BLDCM drives. Specifically, two different controllers are designed based on the dead-beat structure to be switched between conduction and commutation regions. Not only nonideal back-emf signals are considered, but also the variation of back-emf signals in the commutation period is accounted in the controllers. Effect of the commutation delay is addressed in detail and a model-based prediction approach is introduced to reduce this effect. Particularly, the beginning and end points of commutation are predicted according to a dead-beat prediction algorithm. Then this information is utilized to modify PWM duty ratios for the PWM periods common for conduction and commutation periods. The switched controller accounting in all the model properties of the BLDCM drive combined with the commutation delay compensation is the main contribution of this study. In order to validate the performance of the proposed controller, experimental studies are performed and the results show that the proposed method has a significant effect on suppressing commutation torque ripple.

## 2. Mathematical model of BLDCM drive

Figure 1 depicts the equivalent circuit of the BLDCM drive considered in this study. It is assumed that the mutual inductance for each winding and the neutral voltage is zero. In addition, resistance and inductance values of three phases are considered equal in the mathematical model. Thus, the electrical model of the BLDCM drive can be obtained as [17]

$$L \frac{di_{\alpha}}{dt} = v_{\alpha} - Ri_{\alpha} - e_{\alpha} \quad (1)$$

with  $\alpha \in \{a, b, c\}$ , where  $i_a, i_b, i_c$  are phase currents;  $v_a, v_b, v_c$  are the phase voltages;  $e_a, e_b, e_c$  are phase induced back-emfs in stator windings; and  $R$  and  $L$  are the resistance and inductance per phase. The mechanical dynamics of the BLDCM can be given by

$$J \frac{d\omega}{dt} = T_e - T_l - \beta\omega, \quad (2)$$

where  $T_l$  is the load torque, and  $J$  and  $\omega$  are moment of inertia and angular velocity of the rotor, respectively. Torque produced by electrical power is denoted by  $T_e$  and its mathematical expression is given by

$$T_e = \frac{e_a i_a + e_b i_b + e_c i_c}{\omega}. \quad (3)$$

Phase back-emf signals are not assumed to be ideal in this study. Amplitudes of back-emfs are considered to be proportional to the rotor speed. Expressions for back-emfs in terms of rotor speed can be given by

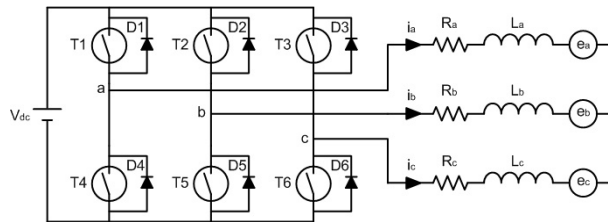


Figure 1. Equivalent BLDCM drive.

$e_a(\theta_e) = f_a(\theta_e)\omega$ ,  $e_b(\theta_e) = f_b(\theta_e)\omega$ , and  $e_c(\theta_e) = f_c(\theta_e)\omega$ , where  $f_a$ ,  $f_b$ , and  $f_c$  are auxiliary functions having the same waveform as corresponding back-emfs and  $\theta_e$  is the electrical rotor angle. Hence, (3) can be modified as

$$T_e = f_a i_a + f_b i_b + f_c i_c. \quad (4)$$

On the other hand, the form of the desired phase currents is determined accordingly to obtain a smooth output torque. Change in normalized back-emf signals measured offline and desired phase currents scaled for a particular level of torque output are illustrated in Figure 2. Utilizing Euler approximation, the difference equations for the electrical model of the BLDCM drive can be obtained as

$$i_\alpha(k+1) = i_\alpha(k) + \frac{T_p}{L} (v_\alpha(k) - R i_\alpha(k) - e_\alpha(k)) \quad (5)$$

considering the rotor speed is fixed between two sampling instances with  $\alpha \in \{a, b, c\}$ , where  $T_p$  denotes sampling period and  $k = 0, 1, 2, \dots$  is the number of sampling instant.

### 3. Reduction of commutation torque ripple

#### 3.1. A brief analysis of BLDCM drives and generalized difference equations

The BLDCM drive is analyzed briefly in this section and interested readers are referred to [6–9] for details. A BLDCM drive has two distinct working regions, namely conduction and commutation periods. In a conduction period only two phases conduct to provide the desired phase currents. On the other hand, a commutation occurs for every  $60^\circ$  electrical degrees and all three phases conduct in a commutation period. One phase of the motor is connected to the supply while another is separated from the supply at the beginning of a commutation period. These phases are called incoming and outgoing phases, respectively. The third phase, whose connection

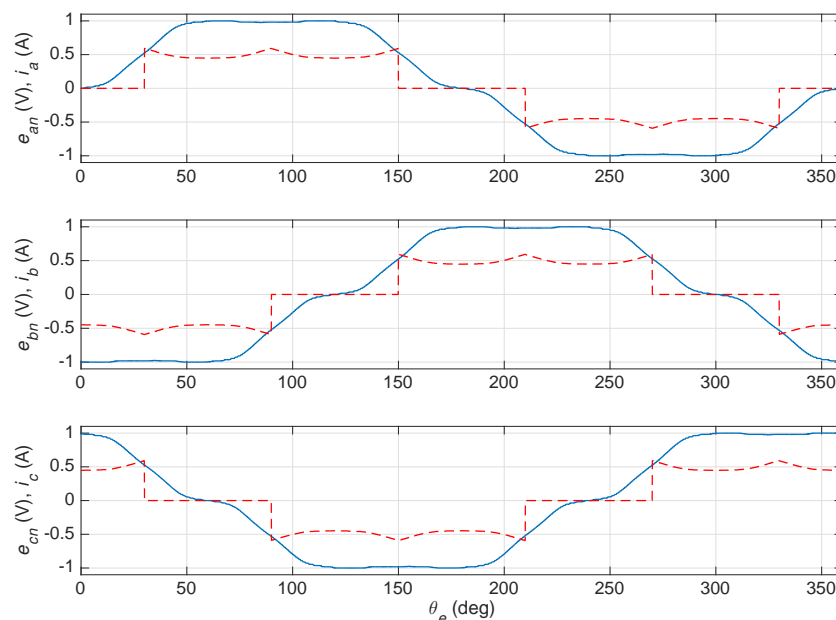


**Figure 2.** Change in the normalized back-emf signals (blue, solid) and corresponding desired phase currents (red, dashed) in one electrical cycle.

is not changed, is said to be the uncommutated phase. A commutation period continues until the outgoing current reaches zero. Outgoing current flows through the inverse parallel diodes and hence it is not possible to reduce the duration of the commutation period. Since the derivative of the outgoing current mainly depends on the amplitude of the back-emfs, low and high speed regions are considered separately in many studies [7]. A commutation period followed by a conduction period is repeated for every  $60^\circ$  electrical degrees, which is defined as a sector. When a commutation occurs, the desired current waveforms for two commutated phases change suddenly (see Figure 2). However, it is clear that the current of a phase cannot be changed suddenly due to the phase inductors. After the occurrence of a commutation, it takes time for the outgoing current to decay to zero, which is called the commutation period. This period leads to a sudden ripple in the torque, which is called commutation torque ripple.

Even though the commutation period cannot be shortened, the aim is to make incoming and outgoing currents track the best possible trajectories for the reduced commutation torque ripple. As a result of that, uncommutated current is controlled for tracking the desired waveform during the commutation. In this manner, conduction and commutation periods are taken into account separately in order to provide the desired uncommutated current. After expressing the mathematical model of both working regions, two different controllers are designed that are switched during the operation. The difference equations of phase currents given in (5) can be organized as

$$i_\alpha(k+1) = i_\alpha(k) + \frac{T_p}{L} \left[ -Ri_\alpha(k) + \frac{1}{3}(v_{\alpha\beta}(k) - e_{\alpha\beta}(k) + v_{\alpha\gamma}(k) - e_{\alpha\gamma}(k)) \right]. \quad (6)$$

for commutation periods where  $\alpha, \beta, \gamma$  stand for the phase indices ( $\alpha, \beta, \gamma \in \{a, b, c\}, \alpha \neq \beta \neq \gamma$ ), and  $v_{xy}$  ( $e_{xy}$ ) is the line to line voltage (induced emf) between the phases  $x$  and  $y$  ( $x, y \in \{\alpha, \beta, \gamma\}, x \neq y$ ). Furthermore, considering that  $\alpha, \beta$ , and  $\gamma$  represent uncommutated, incoming, and outgoing phases, respectively, Eq. (6) can be rewritten as

$$i_\alpha(k+1) = i_\alpha(k) + \frac{T_p}{L} \left[ -Ri_\alpha(k) + v^*(k) - \frac{1}{3}(v_\gamma(k) + e_{\alpha\beta}(k) + e_{\alpha\gamma}(k)) \right]. \quad (7)$$

Here  $v^*$  is regarded as the control input and  $v_\gamma$  is a constant with a sign depending on the direction of the outgoing current since this phase is connected to the supply via a free-wheeling diode. On the other hand, the following discrete-time approximation of the dynamical equations is valid for the phase currents in conduction periods:

$$i_\alpha(k+1) = i_\alpha(k) + \frac{T_p}{L} \left[ -Ri_\alpha(k) + v^*(k) - \frac{1}{2}e_{\alpha\beta}(k) \right]. \quad (8)$$

Note that it is considered in this paper that there are two active phases in conduction periods. The current of the third phase vanishes at the end of the commutation period and then stays at zero until the next commutation.

### 3.2. Controller design

Note that the form of the output torque given in (4) depends on the form of phase currents and corresponding back-emfs. Therefore, the errors between phase currents and their desired signals have to be minimized in order to obtain a smooth output torque. One way to achieve that is to control the uncommutated current during the operation, which is aimed in this study. The mathematical models for conduction and commutation periods are given in (7) and (8). It is worth mentioning at this point that the switch between the mathematical models

of BLDCM during the operation has to be taken into account by the controller. Otherwise the commutation torque ripple may not be mitigated effectively. Thus, two different controllers are designed for conduction and commutation periods separately, and they are switched during the operation.

Let  $i^*(k)$  be the reference current value for  $k$ th time instance regarding the desired output torque, and let

$$e(k) = i_\alpha^*(k) - i_\alpha(k) \quad (9)$$

define the current error. Taking the difference equations given in (7) and (8) into account, one can obtain error difference equations for conduction and commutation periods as

$$e(k+1) = i_\alpha^*(k+1) - i_\alpha(k) - \frac{T_p}{L} [-Ri_\alpha(k) + v^*(k) - \eta(k)]. \quad (10)$$

with

$$\eta(k) = \begin{cases} \frac{1}{3}(v_\gamma(k) + e_{\alpha\beta}(k) + e_{\alpha\gamma}(k)) & , i_\gamma \neq 0 \\ \frac{1}{2}e_{\alpha\beta}(k) & , i_\gamma = 0 \end{cases} . \quad (11)$$

The designed controller regulating the phase current is given by

$$v^*(k) = Ri_\alpha(k) + \eta(k) + \frac{L}{T_p} (i_\alpha^*(k+1) - i_\alpha(k) - \xi(k)) \quad (12)$$

with the assumption that  $i^*(k+1)$  is known for all  $k$  and with  $\xi(k)$  to be assigned. Note that placing (12) into (10) gives

$$e(k+1) = \xi(k), \quad (13)$$

and hence  $v^*(k)$  given in (12) becomes the dead-beat controller when  $\xi(k) = 0$  is satisfied. However, the fragility of the dead-beat controller to model uncertainties and measurement noises is a well-known issue. Moreover, the positive effect of the integral action is also well known to be a practical solution for the application drawbacks such as steady-state errors. In order to attenuate the undesired effect of the uncertainties, the integral action is added to the controller exploiting  $\xi(k)$ . In this manner,  $\xi(k)$  is assigned as follows:

$$\xi(k) = \sum_{n=1}^k e(n). \quad (14)$$

### 3.3. Compensation of commutation delay

The reference phase voltage for the current regulation or reference signal tracking is given in (12). However, the computed reference voltage is not applied directly to the phase coils in a practical application. Instead, the equivalent voltage is generated by the utilization of a PWM signal with a fixed frequency. PWM duty is computed and sent before the corresponding PWM period begins. Hence the applied signal is determined for either a conduction or commutation period. Therefore, the reference voltage for a conduction (commutation) period may also be applied in a commutation (conduction) period since the beginning (end) of a commutation may occur at any point in a PWM period. For instance, after the reference voltage is determined by (12) for a conduction period, let the application of the equivalent control signal be started utilizing PWM. If the commutation occurs in the same PWM period, then the control signal computed for conduction is applied also in the commutation period since PWM duty is fixed until the next PWM period. This issue is illustrated in

Figure 3. The phase voltage determined for the conduction period before the  $(k + 1)$ st period is applied until the next period even though the model is changed by the commutation between  $(k + 1)$ st and  $(k + 2)$ nd periods. Similarly, the control signal applied in the  $(k + 4)$ th PWM period cannot be modified until the next period, although the commutation ends between the  $(k + 4)$ th and  $(k + 5)$ th periods. The term *mixed period* is used for the PWM periods in which the model switches from conduction to commutation or vice versa. Note that two mixed periods may occur in a sector. This inconvenient situation causes undesired ripples in the phase currents especially at the beginning and at the end of commutation periods. Therefore, the output torque is also affected by mixed periods negatively. In order to attenuate this effect, a weighting average of the control signals determined for both conduction and commutation models can be used. However, the beginning and ending points of a commutation period have to be known precisely to compute the weighting average. If this information can be obtained, then one can determine the contributions of the conduction and the commutation periods in the mixed period, and the modified PWM duty can be computed for the mixed period accordingly.

In order to predict the time to the next commutation period, the following equation is utilized assuming the rotor speed is constant between two time instants:

$$\theta_{e_c} = \theta_e(k) + P\omega T_c, \tag{15}$$

where the constant  $\theta_{e_c}$  is the electrical angle for the beginning of the commutation,  $P$  is the number of pole pairs and  $T_c$  is the time duration to the next commutation. Moreover, the intensity of the commutation period in a mixed period can be determined as

$$\rho_1 = \frac{T_p - T_c}{T_p} = 1 - \frac{\theta_{e_c} - \theta_e(k)}{PT_p} \tag{16}$$

for the beginning of the commutation period, where  $T_p$  denotes the PWM period.

On the other hand, the time remaining for the end point of the commutation period can also be computed utilizing the current dynamics. Note that the difference equation for the outgoing current, say  $i_\gamma$ , can be obtained from (6) as

$$i_\gamma(k + 1) = i_\gamma(k) + \frac{T_p}{L} \left[ -Ri_\gamma(k) + \frac{1}{3} (v_{\gamma\alpha}(k) - e_{\gamma\alpha}(k) + v_{\gamma\beta}(k) - e_{\gamma\beta}(k)) \right]. \tag{17}$$

Moreover, since the commutation period ends when the outgoing current reaches zero,

$$T_u \approx \frac{Li_\gamma(k)}{Ri_\gamma(k) - \frac{1}{3} (v_{\gamma\alpha}(k) - e_{\gamma\alpha}(k) + v_{\gamma\beta}(k) - e_{\gamma\beta}(k))} \tag{18}$$

can be derived, where  $T_u$  denotes the duration for the end of the commutation period. Similar to the beginning of the commutation period, one can obtain the intensity of the commutation period in such a mixed period as

$$\rho_2 = \frac{T_u}{T_p} = \frac{Li_\gamma(k)}{T_p [Ri_\gamma(k) - \frac{1}{3} (v_{\gamma\alpha}(k) - e_{\gamma\alpha}(k) + v_{\gamma\beta}(k) - e_{\gamma\beta}(k))]} \tag{19}$$

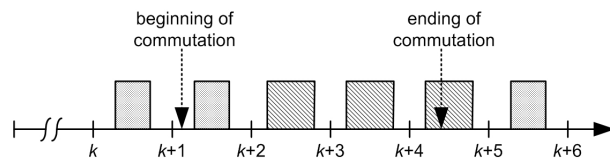


Figure 3. An example for mixed PWM periods.

The aforementioned predictive computations permit one to specify a possible upcoming mixed period. Moreover, the ratio of the time duration between the commutation period and the PWM period can also be determined by these computations. Let  $v_c^*$  and  $v_u^*$  be defined as the reference voltages obtained by (12) for commutation and conduction periods, respectively. Then the reference voltage for a mixed period can be obtained as

$$v_m^* = v_u^*(1 - \rho_i) + v_c^*\rho_i, \quad i = 1, 2. \quad (20)$$

Consequently, the proposed controller consists of three different switched signals given in (12) with (14) and (20) to be implemented in conduction, commutation, and mixed periods.

#### 4. Experimental results

A 75-W BLDCM with 2 pole pairs and 24-V rated voltage has been used to test the viability of the proposed control method. Stator resistance and inductance values of the tested motor for each phase are  $0.58\Omega$  and 2.5 mH, respectively. In order to fix the rotor speed, a 125-W PMSM has been attached to the test motor. A 500-ppr incremental encoder with 2 channels has been utilized to obtain rotor position and rotor speed. Three-phase voltage-fed inverters have been used with 24-V supply voltages to generate necessary phase voltages. The convenient upper (lower) switch of the inverter is driven by PWM signal while the convenient lower (upper) switch is closed during the operation. All other switches have been held open. A 32-bit floating point DSP with 90-MHz operation speed has been used to obtain necessary measurements, to run the control algorithms, and to generate signals for inverters. PWM frequency has been set to 10 kHz with 25 ns resolution. Current measurements have been obtained via Hall effect current sensors for two phases, while the current of the third phase has been computed from these measurements. Analogue measurements have been converted to digital values via 12-bit A/D converter modules of DSP. Phase currents have been sampled 10 times between the middle points of two successive PWM periods simultaneously. Then the average values of measurements have been used in computations. After the phase currents were obtained, the control signals and PWM duty have been determined for the next period. Hence, measurement delay is equal to a PWM period. All the presented results have been measured and saved through an oscilloscope.

Measurement or computation delays are inevitable in practical applications in discrete time. Combined with PWM switching, delays affect the operation in motor drives adversely. Note that there are components for  $k$ th time instance in the control signal given in (12), but it is not possible to obtain the measurements, to compute the control signal, or to send it for generating PWM signal instantaneously for  $k$ th time instance. Hence, the values of the signals used in the controller have to be known before a necessary amount of time from  $k$ th time instance. In this manner, the dead-beat prediction scheme is utilized to approximate the signal values for the beginning of the next PWM period (see [18] for details). All the signals with measurement delay are predicted during the operation.

Various experiments under different working regions have been performed in order to test the proposed control structure under different conditions. In particular, experimental studies for 0.1 Nm and 0.15 Nm desired torque output have been implemented for 750 rpm and 1200 rpm. The results have been saved for three different controllers:

C#1: Nonswitched controller in which the commutation period is not considered.

C#2: Switched controller in which the controllers are switched in conduction and commutation periods without commutation delay compensation.

C#3: Proposed controller in which conduction and commutation periods are taken into account separately with commutation delay compensation.

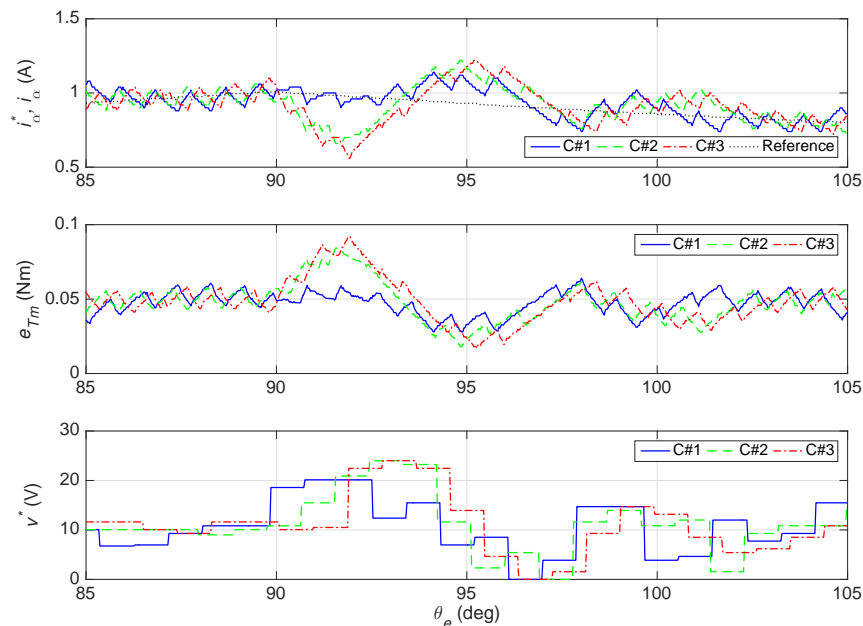
**Table 1.** Maximum error on the output torque.

| Controller        | 750 rpm |         | 1200 rpm |         |
|-------------------|---------|---------|----------|---------|
|                   | 0.1 Nm  | 0.15 Nm | 0.1 Nm   | 0.15 Nm |
| Nonswitched (C#1) | 0.0422  | 0.0331  | 0.0428   | 0.0524  |
| Switched (C#2)    | 0.0344  | 0.0302  | 0.0290   | 0.0354  |
| Proposed (C#3)    | 0.0221  | 0.0216  | 0.0278   | 0.025   |

**Table 2.** RMS value of the output torque error.

| Controller        | 750 rpm |         | 1200 rpm |         |
|-------------------|---------|---------|----------|---------|
|                   | 0.1 Nm  | 0.15 Nm | 0.1 Nm   | 0.15 Nm |
| Nonswitched (C#1) | 0.0145  | 0.0139  | 0.0142   | 0.0207  |
| Switched (C#2)    | 0.0130  | 0.0128  | 0.0113   | 0.0136  |
| Proposed (C#3)    | 0.0081  | 0.0073  | 0.0104   | 0.0079  |

The results of the experiments are given in Figures 4–7. In each figure, uncommutated current with its reference ( $i_\alpha, i_\alpha^*$ ), torque error ( $e_{T_m}$ ), and control signal ( $v^*$ ) are depicted for each controller. The contribution of the proposed controller is clear for each experiment. Even though the response is improved with the switched controller compared to the nonswitched one, the best response is obtained with the proposed controller. This issue is less effective in some cases (see Figure 5), which can be caused by the starting point of the commutation in a sampling period. It is worth mentioning that the proposed controller has no difference from the switched controller if the switch occurs around a point when sampling period begins. To present the effectiveness of the proposed controller further, numerical values for maximum error on the output torque and RMS value of the output torque error are given in Table 1 and Table 2. Numerical results show that the performance is improved with the proposed controller compared to the others for each working condition.

**Figure 4.** Experimental results of C#1 (red, dash-dot), C#2 (green, dashed), and C#3 (blue, solid) for 0.1 Nm output torque with 750 rpm rotor speed.

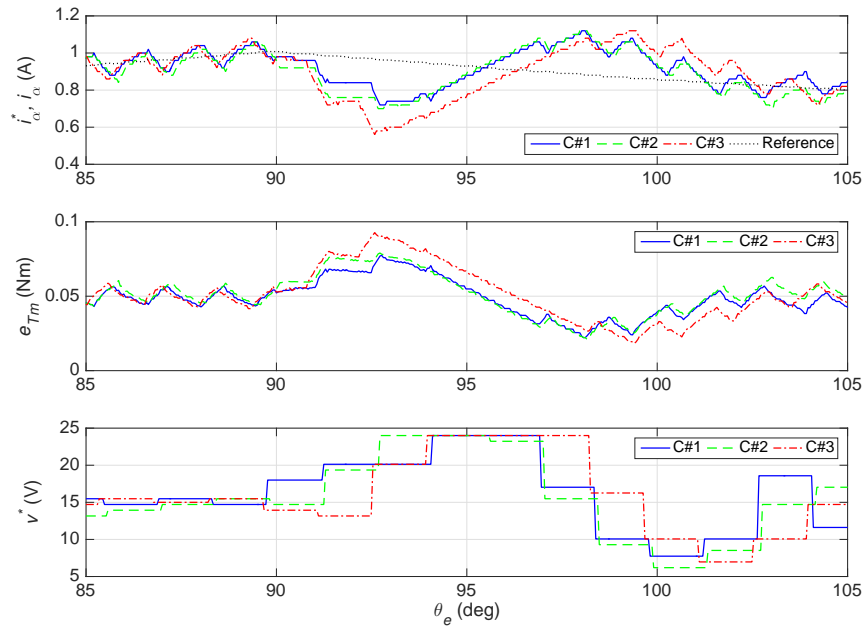


**Figure 5.** Experimental results of C#1 (red, dash-dot), C#2 (green, dashed), and C#3 (blue, solid) for 0.1 Nm output torque with 1200 rpm rotor speed.

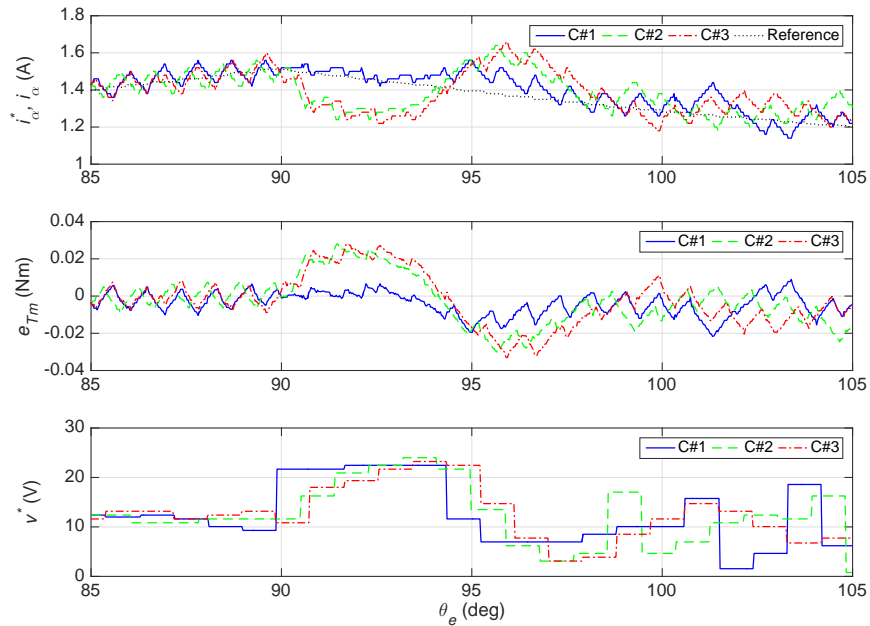


**Figure 6.** Experimental results of C#1 (red, dash-dot), C#2 (green, dashed), and C#3 (blue, solid) for 0.15 Nm output torque with 750 rpm rotor speed.

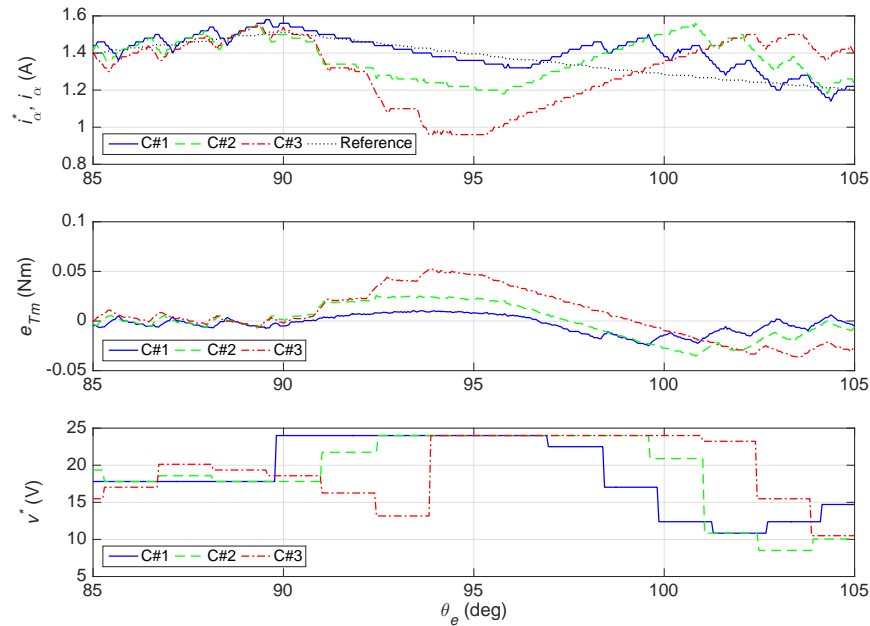


**Figure 7.** Experimental results of C#1 (red, dash-dot), C#2 (green, dashed), and C#3 (blue, solid) for 0.15 Nm output torque with 1200 rpm rotor speed.

## 5. Conclusion

A discrete-time switched controller has been proposed to reduce the commutation torque ripple in BLDCM drives. In addition, a novel method has been introduced to decrease the adverse effect of commutation delay based on a dead-beat prediction algorithm. The overall controller scheme has been tested via comparative experimental studies to show its effectiveness under different working conditions. Compared to the existing methods, the obtained results for the output torque have demonstrated improvement with the proposed controller.

## Acknowledgments

A part of this work was carried out during the MSc study of Ihsan Obayes Khudhair Khudhair in Bahçeşehir University, İstanbul, Turkey. This work was partially supported by the Scientific and Technological Research Council of Turkey (TÜBİTAK) under Grant no. 115E790.

## References

- [1] Buja G, Bertoluzzo M, Keshri RK. Torque ripple-free operation of PM BLDC drives with petal-wave current supply. *IEEE T Ind Electron* 2015; 7: 4034-4043.
- [2] Xia C, Xiao Y, Chen W, Shi T. Torque ripple reduction in brushless DC drives based on reference current optimization using integral variable structure control. *IEEE T Ind Electron* 2014; 2: 738-752.
- [3] Masmoudi M, El Badi B, Masmoudi A. Direct torque control of brushless DC motor drives with improved reliability. *IEEE T Ind Appl* 2014; 6:3744-3753.
- [4] Shi J, Li TC. New method to eliminate commutation torque ripple of brushless DC motor with minimum commutation time. *IEEE T Ind Electron* 2013; 6: 2139-2146.

- [5] Lin YK, Lai YS. Pulsewidth modulation technique for BLDCM drives to reduce commutation torque ripple without calculation of commutation time. *IEEE T Ind Appl* 2011; 4: 1786-1793.
- [6] Carlson R, Lajoie-Mazenc M, Fagundes JCDS. Analysis of torque ripple due to phase commutation in brushless DC machines. *IEEE T Ind Appl* 1992; 3:632-638.
- [7] Salah WA, Ishak D, Zneid BA, Abu\_ALAish A, Jadin MS, Sneineh AA. Implementation of PWM control strategy for torque ripples reduction in brushless DC motors. *Electr Eng* 2015; 3: 1-12.
- [8] Jung SY, Kim YJ, Jae J, Kim J. Commutation control for the low-commutation torque ripple in the position sensorless drive of the low-voltage brushless DC motor. *IEEE T Power Electr* 2014, 11: 5983-5994.
- [9] Xia C, Wang Y, Shi T. Implementation of finite-state model predictive control for commutation torque ripple minimization of permanent-magnet brushless DC motor *IEEE T Ind Electron* 2013; 3: 896-905.
- [10] Fang J, Li H, Han B. Torque ripple reduction in BLDC torque motor with nonideal back EMF. *IEEE T Power Electr* 2012; 11:4630-4637.
- [11] Fang J, Li W, Li H. Self-compensation of the commutation angle based on DC-link current for high-speed brushless DC motors with low inductance. *IEEE T Power Electr* 2014; 1: 428-439.
- [12] Kang SJ, Sul SK. Direct torque control of brushless DC motor with nonideal trapezoidal back EMF. *IEEE T Power Electr* 1995; 6: 796-802.
- [13] Ozturk SB, Alexander WC, Toliyat HA. Direct torque control of four-switch brushless DC motor with non-sinusoidal back EMF. *IEEE T Power Electr* 2010; 2: 263-271.
- [14] Fang J, Zhou X, Liu G. Precise accelerated torque control for small inductance brushless DC motor. *IEEE T Power Electr* 2013; 3: 1400-1412.
- [15] Sheng T, Wang X, Zhang J, Deng Z. Torque-ripple mitigation for brushless DC machine drive system using one-cycle average torque control. *IEEE T Ind Electron* 2015; 4: 2114-2122.
- [16] Cui C, Liu G, Wang K. A novel drive method for high-speed brushless DC motor operating in a wide range. *IEEE T Power Electr* 2015; 9: 4998-5008.
- [17] Krashnan R. Permanent Magnet Synchronous and Brushless DC Motor Drives. Boca Raton, FL, USA: CRC Press, 2009.
- [18] Türker T, Buyukkeles U, Mese H, Bakan AF. A discrete-time current controller for permanent magnet synchronous motor drives. In: *41st Annual Conference on IEEE Industrial Electronics Society*; 9-12 November 2015; Yokohama, Japan: pp. 1453-1458.